Conductivity in a symmetry-broken phase: Spinless fermions with $1/d$ corrections

Götz S. Uhrig*
Laboratoire de Physique des Solides, Bâtiment 510, Université Paris-Sud, F-91405 Orsay, France
(Received 12 April 1996)

The dynamic conductivity $\sigma(\omega)$ of strongly correlated electrons in a symmetry-broken phase is investigated in the present work. The model considered consists of spinless fermions with repulsive interaction on a simple cubic lattice. The investigated symmetry-broken phase is the charge density wave (CDW) with wave vector $\mathbf{Q}=(\pi,\pi,\pi)^{\dagger}$ which occurs at half-filling. The calculations are based on the high dimensional approach, i.e., an expansion in the inverse dimension $1/d$ is used. The finite dimensionality is accounted for by the inclusion of linear terms in $1/d$ and the true finite dimensional DOS. Special care is paid to the setup of a conserving approximation in the sense of Baym/Kadanoff without inconsistencies. The resulting Bethe-Salpeter equation is solved for the dynamic conductivity in the nonsymmetry-broken and in the symmetry-broken phase (AB-CDW). The dc-conductivity is reduced drastically in the CDW. Yet it does not vanish in the limit $T\rightarrow 0$ due to a subtle cancellation of diverging mobility and vanishing DOS. In the dynamic conductivity $\sigma(\omega)$ the energy gap induced by the symmetry breaking is clearly discernible. In addition, the vertex corrections of order $1/d$ lead to an excitonic resonance lying within the gap. [S0163-1829(96)07140-8]

I. INTRODUCTION

The investigation of the transport properties of highly correlated fermionic systems has attracted much attention in recent years. A thorough understanding of the conductivity in particular is essential for the technical application of materials such as metallic oxides in electronic devices. The development of a new analytic approach, the limit of infinite dimension for fermionic systems,[1,2] allowed the numerical description of the metal-insulator occurring in the half-filled Hubbard model in $d=\infty$ for higher values of the interaction U assuming a homogeneous phase. [3,4] The latter assumption means that one deliberately ignores the possible occurrence of symmetry breaking for the sake of simplicity. It is argued that on frustrated lattices symmetry breaking is suppressed so that the metal-insulator transition occurs at higher temperatures than those at which symmetry breaking sets in.

With this background in mind, it is the aim of this work to extend and to complement the results known so far into two directions. First, the finite dimensionality of realistic systems, i.e., mostly $d=3$, shall be included at least to lowest nontrivial order in an expansion in $1/d$. Much care is used in including these corrections without physical and/or analytic inconsistencies. It is shown that it is *not* sufficient to use a conserving, Φ-derivable approximation in the sense of Baym/Kadanoff. Furthermore, the true three-dimensional DOS will be used. Second, the influence of symmetry breaking on the conductivity, especially the question of possible metal-insulator transitions induced by symmetry breaking, shall be investigated.

To this end, the model of spinless fermions with repulsive interaction for particles on adjacent sites is considered on a generic bipartite lattice, namely the simple cubic lattice. Its Hamiltonian at half-filling $n=1/2$ reads

$$\hat{H}=-\frac{t}{\sqrt{Z}}\sum_{\langle i,j\rangle}\hat{c}_i^{+}\hat{c}_j+\frac{U}{2Z}\sum_{\langle i,j\rangle}\hat{n}_i\hat{n}_j-\frac{U}{2}\sum_i\hat{n}_i, \qquad (1)$$

where $\hat{c}_i^{+}(\hat{c}_i)$ creates (annihilates) a fermion at site i. The sum $\Sigma_{\langle i,j\rangle}$ runs over all sites i and j which are nearest neighbors. The coordination number $Z=2d=6$ appears for the proper scaling of the kinetic energy[1] and for the proper scaling of the potential energy.[5] The interaction constant is U.

In this model the symmetry is broken yielding an AB-CDW at half-filling[6] for infinitesimal values of the interaction at $T=0$ and for sufficiently large interaction at all finite temperatures. The AB-CDW consists of alternating sites with a particle density above (below) average. The order parameter b is the absolute deviation of the particle density from its average.[6] As far as the occurrence of a symmetry-broken phase is concerned, the model of spinless fermions at half-filling is similar to the Hubbard model at half-filling which displays antiferromagnetic behavior. The main differences are that the broken symmetry for spinless fermions is discrete whereas it is continuous in the Hubbard model, and the fact that a local interaction like the one in the Hubbard model does not favor a spatial order by itself. The latter fact leads to a value of $T_c\propto 1/U$ for large U in the Hubbard model whereas one has $T_c\propto U$ in the spinless fermions model.

The paper is organized as follows. Succeeding this Introduction it is discussed how a thermodynamically and analytically consistent extension of the limit $Z\rightarrow\infty$ can be performed. Next the basic equations for the extension to linear order $1/Z$ are derived and their numerical evaluation is sketched. This third section contains also results for the DOS and the corresponding proper self-energy. In Sec. IV the Bethe-Salpeter equation is set up and solved for the conductivity $\sigma(\omega)$. The preservation of the f-sum rule is discussed. Numerical results for the dc and the ac conductivity are presented in Sec. V. The findings are summarized and discussed in the final section.

All energies (temperatures, respectively) throughout this paper will be given in units of the root-mean-square of the ''free,'' i.e., noninteracting, density-of-states of the lattice model concerned. All conductivities will be given in units of

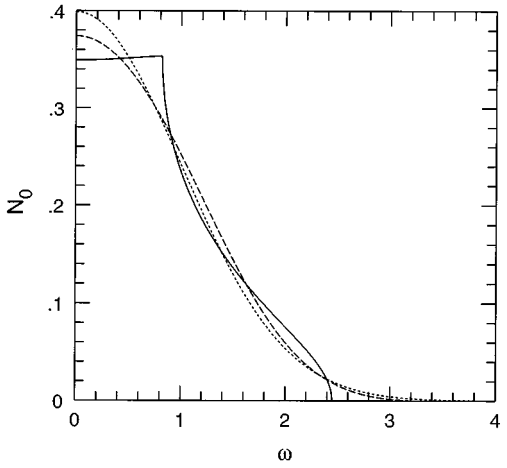

FIG. 1. Noninteracting DOS in $d=\infty$ (short-dashed curve), in $d=3$ (solid curve), and the DOS expanded in $1/d$ evaluated in $d=3$ (long-dashed curve). These densities of states are symmetric about the y axis.

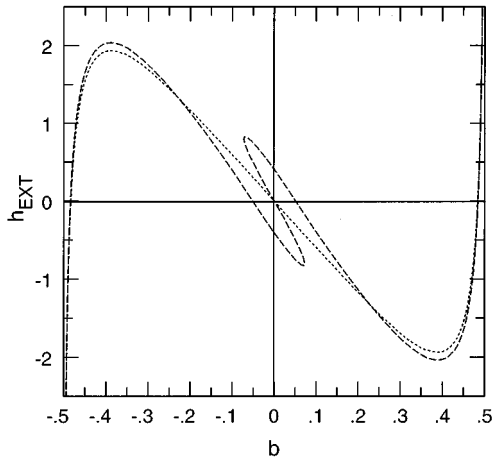

FIG. 2. Externally applied field h_{EXT} as a function of the order parameter b for $U=9$ and $T=0$ in $d=3$. The short-dashed curve depicts the $1/d$ self-consistent result, the long-dashed curve the result of a systematic expansion of the self-energy. The zeros of the curves correspond to thermodynamic equilibrium. But only zeros with positive slope are locally stable ($b\approx 0.48$).

$e^2/(\hbar a^{d-2})$, where a is the lattice constant. The constants a, $\hbar$, and k_B (Boltzmann's constant) are set to unity.

II. PROPER SELF-CONSISTENT EXTENSION OF $Z=\infty$

In the case $Z=\infty$, the evaluation of diagrams and the treatment of quantities like the DOS are conceptually simple. It is always the leading contribution in $1/Z$ and only this which must be kept. There is no dependence on the sequence in which certain quantities and the equations relating them are considered. All sum rules which hold in any dimension also hold at $Z=\infty$, continuity provided for the limit $Z\to\infty$. This simplicity is lost as soon as corrections in $1/Z$ are to be included. For concreteness, let us consider the linear corrections $1/Z$; the problems are illustrated for the free DOS, the Dyson equation, and the free energy F as a function of the order parameter b.

The DOS is a non-negative function of which the zeroth moment is unity. This holds in any dimension, hence in $Z=\infty$. On including the linear corrections[5] one realizes that the approximate expression becomes negative at large values of ω. This is a disadvantage of the otherwise systematic expansion. Another inconvenience catches the eye in Fig. 1. The expanded DOS does not improve considerably the agreement with the true finite dimensional DOS (here $d=3$). A finite expansion in $1/Z$ cannot produce the van-Hove singularities.

To circumvent the problem of the DOS expansion, we decide to use the exact finite dimensional DOS, i.e., the $d=3$ DOS. This procedure provides often even in $d=1$ a remarkable agreement.[6,7] In $d=3$, this approximation yields qualitative agreement for the local DOS as compared to finite dimensional perturbation results.[8] Presently, the approach of using a finite dimensional DOS in an otherwise infinite dimensional calculation as approximation for the finite dimensional problem is employed as so-called ''dynamical mean-field theory''[4] or ''local impurity self-consistent approximation.''[3]

Next the problem of a systematic $1/Z$ expansion is discussed for the Dyson equation. It is stated in a simple case when the self-energy is strictly local in real space, i.e., constant in momentum space,

$$g(\omega)=g_0(\omega-\Sigma(\omega)). \tag{2}$$

This case is realized, for instance, in the Hubbard model in $d=\infty$.[5,9] No lattice site or spin index appears since the phase is assumed to be homogeneous and nonmagnetic. The quantity $g(\omega)$ stands for the full local Green function $G_{i,i}(\omega)$ and $g_0(\omega)$ stands for the free Green function $G_{0;i,i}(\omega)$. The expansion of the Green function corresponds to the expansion of the thermodynamic potential since they depend linearly on each other.[10] An expansion of the self-energy, however, yields a *different* expression for $g(\omega)$ since $g_0(\omega)$ is not a linear function. The expansion of the self-energy seems more promising since it preserves the Dyson equation by construction. Moreover, it is able to describe the shift of singularities, e.g., the shifts of the band edges. (Note that we discuss here finite expansions of the quantities considered.)

In spite of the choice to expand the self-energy some ambiguity persists. In Fig. 2, this problem is illustrated. It arises in the description of spontaneous symmetry breaking. Two results for the dependence of the conjugated field on the order parameter are opposed. The data refer to the AB-CDW occurring in the spinless fermion problem at half-filling. The dotted curve results from a fully self-consistent calculation whereas the dashed curve results from a systematic expansion of the self-energy. Note that the self-consistent approach generates higher order contributions.

The argument results now from the strange behavior of the dashed curve in the vicinity of the origin. The free energy belonging to the dotted curve can be found by integration; it has an unstable maximum ($\partial h_{\mathrm{EXT}}/\partial b<0$) at $b=0$ and two stable minima ($\partial h_{\mathrm{EXT}}/\partial b>0$) at $b\approx\pm 0.48$. But there is no free energy belonging to the dashed curve since it would have three maxima in sequence around $b=0$ which is mathematically impossible (theorem of Rolle). This is a very strong argument in favor of a self-consistent calculation.

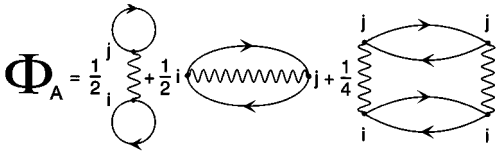

FIG. 3. Diagrams contained in $\Phi_A[G]$. The first generates the Hartree term, the second the Fock term, and the third the local correlation term. The solid lines represent dressed propagators, the wavy lines the interactions. The sum runs over the lattice sites i,j.

For completeness, it shall be mentioned that one may argue that in the vicinity of the physical solutions, i.e., the minima, the difference of both approaches is negligible. There are also cases known where the systematic, non-self-consistent approach yields better results.[11] But there is still another advantage of the self-consistent treatment which will be crucial for what follows. In the sense of Baym/Kadanoff[12,13] it covers also the calculations of two-particle properties and ensures the preservation of sum rules. So, Schweitzer and Czycholl resorted in their calulation of resistance and thermopower for the periodic Anderson model to the self-consistent treatment[14] although their results for the local DOS did not necessarily favor this approach.[11]

As a result of the above discussion the starting point for the inclusion of $1/Z$ corrections is the generating functional Φ according to Baym/Kadanoff.[12,13] This is the quantity which is expanded in a $1/Z$ series. Then the truncation of this series yields an approximation to the corresponding order. The power counting for the diagrams of Φ has been explained previously.[6,15] Here it shall just be stated that the first diagram in Fig. 3 is of order $\mathcal{O}(1)$ and the two other diagrams in Fig. 3 produce the linear corrections $\mathcal{O}(1/Z)$ whereas the diagrams in Fig. 4 are examples for $\mathcal{O}(1/Z^2)$ contributions. Thus Fig. 3 visualizes the approximate Φ_A potential which will be used in this work.

By functional derivation the self-energy shown in Fig. 5 is obtained. Note that the Fock diagram is seemingly of another order, namely $\mathcal{O}(1/Z^{3/2})$, than the third diagram, $\mathcal{O}(1/Z)$, which is called the local correlation diagram henceforth. What matters, however, is the order relative to the free Green function which is $\mathcal{O}(1/Z^{1/2})$ for adjacent sites. It is another advantage of the Baym/Kadanoff formalism that one does not need to bother about these questions once the approximate Φ potential is chosen.

Now a point shall be highlighted which has not been mentioned before to our knowledge. In spite of the many arguments in favor of the Baym/Kadanoff formalism, its naive application does not guarantee the absence of unphysical results. A counter example serves as an illustration. Consider an approximate Φ consisting only of the diagram in Fig. 4(a), summed over all sites i,j,i',j', such that i and j (i' and j', respectively) are adjacent to one another and fulfill $j\neq j'$ and $i\neq i'$. The resulting nearest-neighbor self-energy $\Sigma_{i,j}=t(\omega)=t'(\omega)+it''(\omega)$ has a finite imaginary part $t''(\omega)$. Using the Dyson equation, one obtains in the homogeneous phase

$$G_{\mathbf{k},\mathbf{k}}(\omega+0i)=\frac{1}{\omega+0i-[1+t(\omega+0i)]\varepsilon(\mathbf{k})}$$
$$=\frac{\omega-(1+t')\varepsilon(\mathbf{k})+it''\varepsilon(\mathbf{k})}{[\omega+0i-(1+t')\varepsilon(\mathbf{k})]^2+(t''\varepsilon(\mathbf{k}))^2}.$$

By choosing an appropriate wave vector $\mathbf{k}$ at fixed ω one can have the sign of $\varepsilon(\mathbf{k})$ such that the imaginary part of $G_{\mathbf{k},\mathbf{k}}(\omega+0i)$ is positive.[16] This is a contradiction to the exact result.[10] Note that the details of $t(\omega)$ are not essential as long as the imaginary part is finite.

The counterexample above is not only of academic interest. Schweitzer and Czycholl observed as well that the inclusion of a nearest-neighbor self-energy leads to wrong signs of the imaginary parts. They considered the $1/d$ expansion of a U^2 perturbation theory around Hartree-Fock for the Hubbard model and the periodic Anderson model.[8,17] They reached consistency by including higher $1/d$ corrections (for $d=1$ up to 50 terms).[8] Problems with the analyticity (uniqueness) of the solution occurred also in the first investigations of $1/d$ corrections in the Hubbard model[3] (Falicov-Kimball model[18]).

To the author's knowledge there is no necessary or sufficient theory so far, which predicts under which circumstances such problems have to be expected or can be excluded. A sufficient argument excluding wrong signs of the imaginary part of the approximate self-energy is given by the following theorem.

If the approximation considered can be interpreted as an expansion of the self-energy in a parameter $\lambda\geqslant 0$ and if m is the leading order, in which the imaginary part of the self-energy does *not* vanish, then the self-energy approximated in the mth order has the right sign.

The proof relies on the continuity of limits if the expansion exists. According to the precondition, it holds that

$$0\geqslant \mathrm{Im}\Sigma_\lambda(\omega,\mathbf{k})=\lambda^m\mathrm{Im}\Sigma^{(m)}(\omega,\mathbf{k})+\mathcal{O}(\lambda^{(m+1)}), \quad (3)$$

which is equivalent to

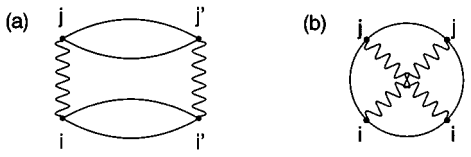

FIG. 4. Two examples of diagrams in higher order (here: quadratic) in $1/Z$. The sites i and j are adjacent as are the sites i' and j'. Additionally, $i\neq i'$ and $j\neq j'$ holds.

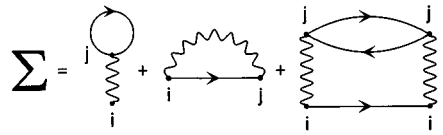

FIG. 5. The self-energy diagrams derived from Fig. 3 by taking out one propagator line. The diagrams shown contribute in order $1/Z$.

$$0 \geqslant \lim_{\lambda \to 0+} \lambda^{-m} \mathrm{Im}\Sigma_\lambda(\omega,\mathbf{k}) = \mathrm{Im}\Sigma^{(m)}(\omega,\mathbf{k}). \tag{4}$$

The index $\mathbf{k}$ is the wave vector in a homogeneous, translationally invariant phase. The derivation for general phases, for instance the AB-CDW, is given in Appendix A.

The derivation in Eq. (3) and in Eq. (4) holds strictly only for the non-self-consistent treatment. In the generic situation, however, the leading order of the self-energy with nonvanishing imaginary part results from a certain diagram class and the analytic properties do not depend on the specific form of the Green function entering. If this is the case, the statement of the theorem extends also to the self-consistent treatment where the quantitative form of the Green functions are not known *a priori*.

The theorem helps one to understand the observations made by Schweitzer and Czycholl. In the $1/d$ expansion of the d-dimensional Hubbard model and of the periodic Anderson model one has $\lambda = 1/d$ and $m = 0$ since the self-energy is imaginary already in the first order. For the perturbation theory in U one has $\lambda = U$ and $m = 2$ since the self-energy stays real in Hartree-Fock. Applying the rationale of the theorem twice one understands that the self-energy in U^2 of the infinite dimensional model has the right analytic behavior. If further $1/d$ corrections are included this does not need to be true. The result of Schweitzer and Czycholl, that the linear $1/d$ correction leads to wrong signs, proves that the theorem is sharp: If the precondition fails, the implication fails, too. The second obervation, that the inclusion of *very many* $1/d$ correction terms remedies the failure, can also be understood easily. In this case the calculations approximate the U^2 perturbation theory of the *finite* dimensional models very well. According to the theorem, this perturbation theory displays the right sign, too.

The above observations indicate that also the analyticity problems encountered for $1/d$ corrections in the Hubbard model[3] are not due to the approximations used to solve the effective impurity problems. Rather, each time that the theorem does not apply one has to expect that analyticity problems arise for certain parameters. Considering Eq. (6a) in Ref. 18 or equivalently Eq. (370) in Ref. 3 one realizes that the spectral density of the local self-energy might change sign. This cannot be excluded obviously from the way in which the impurity self-energies are computed.

Turning to the $1/d$ expansion of the present model of spinless fermions ($\lambda = 1/d$), one notes that the theorem applies with $m = 1$. Therefore, the equations including linear $1/d$ corrections display the right analyticity. These equation will be set up in the following.

A. Resulting equations and one-particle results

This section is kept very concise since it contains material which is partly published elsewhere.[6] For two reasons, however, it cannot be omitted. First, a different notation using different intermediate quantities shall be introduced. Second, the one-particle results are necessary requisites to understand the conductivity results in the subsequent section.

The treatment of a self-energy of the type depicted in Fig. 5 is commonly known (see, e.g., Refs. 11, 19, and 20). Dealing with the symmetry-broken phase, however, requires some extension. In a previous work[6] the local Green function and the self-energy are distinguished according to the sublattice to which they belong. In the present work, sum and difference of the quantities on the two sublattices will be used. The local quantities on site i belonging to sublattice $\tau \in \{A,B\}$ are

$$g_\tau := G_{i,i}(\omega), \tag{5a}$$

$$\Sigma_\tau(\omega) := \Sigma^H_{i,i}(\omega) + \Sigma^C_{i,i}(\omega), \tag{5b}$$

where $G_{i,i}(\omega)$ is the full local Green function and Σ is the local self-energy. The Fock part will be treated subsequently. The index H stands for the Hartree term (first diagram in Fig. 5); the index C stands for the local correlation (third diagram in Fig. 5). Let us define

$$g_S(\omega) := [g_A(\omega) + g_B(\omega)]/2, \tag{6a}$$

$$g_D(\omega) := [g_A(\omega) - g_B(\omega)]/2, \tag{6b}$$

$$\Sigma(\omega) := [\Sigma_A(\omega) + \Sigma_B(\omega)]/2, \tag{6c}$$

$$\Delta(\omega) := [\Sigma_A(\omega) - \Sigma_B(\omega)]/2. \tag{6d}$$

The spectral functions of the Green function are called N_S and N_D, respectively; the spectral functions of the self-energy Σ and Δ are called N_Σ and N_Δ, respectively. The nonlocal Fock term is $\Sigma^F := \Sigma_{i,j}$, where i and j are adjacent sites. It turns out that Σ^F is negative (for repulsive interaction), real, and that it does not depend on whether the fermion hops from A to B or vice versa. Hence, it renormalizes the hopping

$$t \to \gamma t \quad \text{with} \quad \gamma := 1 - \sqrt{Z}\Sigma^F/t. \tag{7}$$

Note that for attractive interaction γ could become 0, which would lead to a breakdown of the theory. Such a singularity is absent in the repulsive case.

In the AB-CDW, the modes at $\mathbf{k}$ couple to those at $\mathbf{k}+\mathbf{Q}$. Hence one has

$$\begin{pmatrix} G_{\mathbf{k},\mathbf{k}} & G_{\mathbf{k},\mathbf{k}+\mathbf{Q}} \\ G_{\mathbf{k}+\mathbf{Q},\mathbf{k}} & G_{\mathbf{k}+\mathbf{Q},\mathbf{k}+\mathbf{Q}} \end{pmatrix} = \begin{pmatrix} \omega - \Sigma(\omega) - \gamma\varepsilon & -\Delta(\omega) \\ -\Delta(\omega) & \omega - \Sigma(\omega) + \gamma\varepsilon \end{pmatrix}^{-1}. \tag{8}$$

From this equation one obtains

$$g_S(\omega) = \frac{w}{\gamma\sqrt{w^2 - \Delta^2(\omega)}} g_0\left(\sqrt{w^2 - \Delta^2(\omega)}/\gamma\right) = \int_{-\infty}^{\infty} \frac{w}{w^2 - (\gamma\varepsilon)^2 - \Delta^2} N_0(\varepsilon)\, d\varepsilon, \tag{9a}$$

$$g_D(\omega) = \frac{\Delta(\omega)}{\gamma\sqrt{w^2 - \Delta^2(\omega)}} g_0\left(\sqrt{w^2 - \Delta^2(\omega)}/\gamma\right) = \int_{-\infty}^{\infty} \frac{\Delta}{w^2 - (\gamma\varepsilon)^2 - \Delta^2} N_0(\varepsilon)\, d\varepsilon, \tag{9b}$$

where w is shorthand for $\omega - \Sigma(\omega)$.

The averaged Hartree term $U(n_A+n_B)/2$ renormalizes the chemical potential.[15] The Hartree contribution to Δ is Ub, where $b:=(n_B-n_A)/2$ is the order parameter, i.e., the particle density difference. It is given by $b=-\int_{-\infty}^{\infty}N_D(\omega)f_F(\omega)d\omega$, where $f_F(\omega)$ is the Fermi function.

The Fock term can be calculated from the nearest-neighbor Green function $G_{j+a,j}$,

$$\Sigma^F=\frac{U}{\pi Z}\int_{-\infty}^{\infty}\mathrm{Im}(G_{j+a,j}(\omega+0i))f_F(\omega)d\omega, \tag{10}$$

which is given by

$$\begin{aligned}G_{j+a,j}(\omega)&=-\frac{1}{\sqrt{Z}}\int_{\mathrm{BZ}}\varepsilon(\mathbf{k})G_{\mathbf{k},\mathbf{k}}\frac{dk^d}{(2\pi)^d}\\&=-\frac{1}{\gamma\sqrt{Z}}[(\omega-\Sigma)g_S(\omega)-\Delta g_D(\omega)]d\varepsilon.\end{aligned} \tag{11}$$

The Fock term is related to the kinetic energy $\Sigma^F=(U/Z^{3/2})\langle\hat{T}\rangle$. Thus, Eq. (10) can be evaluated using Eqs. (11) and (9).

The local correlation term is given in terms of the Matsubara frequencies ω_λ (fermionic) and ω_l (bosonic) by

$$\Sigma_\tau^C(i\omega_\nu)=-\frac{U^2T^2}{Z}\sum_{l,\lambda}g_{\bar{\tau}}(i\omega_\lambda+i\omega_l)g_{\bar{\tau}}(i\omega_\lambda)g_\tau(i\omega_l+i\omega_\nu). \tag{12}$$

Here, the index $\bar{\tau}$ stands for the *other* sublattice, i.e., for A if $\tau=B$ and vice versa. By performing the Matsubara sum one obtains the convolution

$$\begin{aligned}N_{\Sigma_\tau}(\omega)=\frac{U^2}{Z}\int_{-\infty}^{\infty}\int_{-\infty}^{\infty}&N_{\bar{\tau}}(\omega'')N_{\bar{\tau}}(\omega''-\omega')\\&\times N_\tau(\omega-\omega')\cdot[f_F(\omega'-\omega)f_F(-\omega'')f_F(\omega''-\omega')\\&+f_F(\omega-\omega')f_F(\omega'')f_F(\omega'-\omega'')]d\omega'd\omega''\end{aligned} \tag{13}$$

for the spectral function $N_{\Sigma_\tau}(\omega)$ belonging to $\Sigma_\tau^C(\omega)$. The convolution can be expressed most conveniently in the Fourier transforms

$$\widetilde{N}^{\pm}(t):=\int_{-\infty}^{\infty}\exp(-i\omega t)N(\pm\omega)f_F(-\omega), \tag{14a}$$

$$\widetilde{N}(t):=\int_{-\infty}^{\infty}\exp(-i\omega t)N(\omega). \tag{14b}$$

Equation (13) becomes as simple as $\widetilde{N}_{\Sigma_\tau}(t)=U^2/Z[\widetilde{N}_{\bar{\tau}}^{+}\widetilde{N}_{\tau}^{+}\widetilde{N}_{\bar{\tau}}^{-}|_t+\widetilde{N}_{\bar{\tau}}^{-}\widetilde{N}_{\tau}^{-}\widetilde{N}_{\bar{\tau}}^{+}|_{-t}]$. In sums and differences one obtains

$$\begin{aligned}\widetilde{N}_\Sigma(t)=\frac{U^2}{Z}[&\{(\widetilde{N}_S^+)^2-(\widetilde{N}_D^+)^2\}\widetilde{N}_S^-|_t\\&+\{(\widetilde{N}_S^+)^2-(\widetilde{N}_D^+)^2\}\widetilde{N}_S^+|_{-t}]\end{aligned} \tag{15a}$$

$$\begin{aligned}\widetilde{N}_\Delta(t)=-\frac{U^2}{Z}[&\{(\widetilde{N}_S^+)^2-(\widetilde{N}_D^+)^2\}\widetilde{N}_D^-|_t\\&+\{(\widetilde{N}_S^+)^2-(\widetilde{N}_D^+)^2\widetilde{N}_D^+|_{-t}.\end{aligned} \tag{15b}$$

The complete self-energy Σ and Δ are given by the following inverse Fourier transforms:

$$\Sigma(\omega+0i)=-i\int_0^{\infty}\exp(i\omega t-0t)\widetilde{N}_\Sigma(t)dt, \tag{16a}$$

$$\Delta(\omega+0i)=Ub-i\int_0^{\infty}\exp(i\omega t-0t)\widetilde{N}_\Delta(t)dt. \tag{16b}$$

In Eq. (16b) the Hartree part has been added.

So far, no assumptions concerning the DOS entered. The formulas hold for all fillings. At the particular value of half-filling the additional symmetries $N_S(\omega)=N_S(-\omega)$, $N_D(\omega)=-N_D(-\omega)$, $N_\Sigma(\omega)=N_\Sigma(-\omega)$, and $N_\Delta(\omega)=-N_\Delta(-\omega)$ can be exploited. The fact that the spectral densities are real tells us that $\widetilde{N}(-t)$ is the complex conjugate (c.c.) of $\widetilde{N}(t)$. Thus Eq. (15) simplifies at half-filling to

$$\widetilde{N}_\Sigma(t)=\frac{U^2}{Z}[\{(\widetilde{N}_S^+)^2-(\widetilde{N}_D^+)^2\}\widetilde{N}_S^+|_t+\text{ c.c.}], \tag{17a}$$

$$\widetilde{N}_\Delta(t)=\frac{U^2}{Z}[\{(\widetilde{N}_S^+)^2-(\widetilde{N}_D^+)^2\}\widetilde{N}_D^+|_t-\text{ c.c.}]. \tag{17b}$$

This terminates the setup of the equations which have to be solved self-consistently on the one-particle level.

For those who intend to implement these equations or similar ones some remarks on the numerical realization are in order. As usual, the self-consistent set of equations is solved by iteration. At $T=0$ it is favorable to use a relaxed iteration. This means that the self-energy Σ and Δ from the nth and from the $n+1$ iteration are averaged and used for the subsequent calculation instead of using only the $n+1$ iteration. This procedure damps oscillatory deviations from the fixed point more rapidly. It is even more advantageous to let the programme decide whether relaxed or nonrelaxed iteration converges faster.

The Fourier transformation is the most time consuming step. The best algorithm for this task is the so-called fast Fourier transformation (FFT). The extremely large number of points, which can be used with the FFT, overcompensates the disadvantage of an equidistant mesh which cannot be adapted to regions where the DOS changes rapidly.[6] In the AB-CDW 2^{19} points were used. The vectorization on an IBM3090 still permitted us to do one iteration step comprising four FFT in 19 sec. A very good precision could be achieved. The sum rules

$$\int_0^{\infty}N_\Sigma(\omega)d\omega=\frac{U^2}{Z}\frac{1}{2}\left(\frac{1}{4}-b^2\right), \tag{18a}$$

$$\int_0^{\infty}N_\Delta(\omega)d\omega=\frac{U^2}{Z}b\left(\frac{1}{4}-b^2\right), \tag{18b}$$

are preserved up to 10^{-6}. Note that Eq. (18b) holds only at $T=0$ whereas Eq. (18a) holds for all temperatures.

In order to achieve the high precision also at $T=0$, it is necessary to discretize the DOS carefully. At the gap edges the DOS displays inverse square root divergences $a/\sqrt{\omega-\omega_\Delta}$. The parameters a and ω_Δ are determined directly from the self-energy using Eq. (9). The diverging part of the DOS is discretized by using the average value in the interval $[\omega_i-\delta\omega/2,\omega_i+\delta\omega/2]$ instead of the DOS value at ω_i.

Once the Fourier transforms are essentially linear one has to avoid a nonlinear time loss in the calculation of the complex free Green function $g_0(z)$. Therefore, the integration from the Hilbert representation must be avoided. This is done by using the approximate expression

$$N_3(\varepsilon)\approx\frac{1}{\pi}\Bigg[\left\{\frac{13033}{29088}+\frac{8675}{174528}\varepsilon^2\right\}\sqrt{6-\varepsilon^2}-\left\{\frac{4167}{6464}+\frac{459}{6464\sqrt{6}}\varepsilon+\frac{729}{12928}\varepsilon^2\right\}\sqrt{2/3-(\varepsilon-2\sqrt{2/3})^2}-\left\{\frac{4167}{6464}-\frac{459}{6464\sqrt{6}}\varepsilon+\frac{729}{12928}\varepsilon^2\right\}\sqrt{2/3-(\varepsilon+2\sqrt{2/3})^2}\Bigg], \tag{19}$$

for the three-dimensional DOS $N_3(\varepsilon)$. The identities $h(z;a):=(1/\pi)\int_{-\sqrt{a}}^{\sqrt{a}}\sqrt{a-\varepsilon^2}/(z-\varepsilon)d\varepsilon=z\pm\sqrt{z^2-a}$ and $(1/\pi)\int_{-\sqrt{a}}^{\sqrt{a}}\varepsilon\sqrt{a-\varepsilon^2}/(z-\varepsilon)d\varepsilon=-(a/2)+zh(z;a)$ permit us to compute $g_0(z)$ for any z quickly. The right-hand side (rhs) of Eq. (19) is chosen such that the van-Hove singularities are at the right places and such that the first moments (including the eighth) are reproduced exactly. The relative accuracy achieved is 4×10^{-4} for $N_3(0)$ and 10^{-5} for the 10th and the 12th moment.

The calculations of the Hartree and of the Fock parts are linear in the number of discretization points. Concluding the remarks on the numerical realization we state that all parts of an iteration step are essentially linear in the number of points used. This allows a reliable and efficient computation.

In Fig. 6, results for the DOS and the spectral density of the self-energy in the homogeneous phase are shown. The spontaneous symmetry breaking is deliberately suppressed. Only positive frequencies are displayed since the functions are even. At $T=0$, one notes that the imaginary part of the self-energy tends quadratically to zero for $\omega\to0$. From Eq. (13) this follows for all free DOS with finite nonsingular value at the Fermi edge. Thus the homogeneous low temperature phase of interacting spinless fermions is a Fermi liquid. But this phase is thermodynamically unstable (see below). The DOS still bears signs of the van-Hove singularities which are smeared out only a little due to the interaction. Note that the width is increased by the Fock term. In the free case the half-width is $\sqrt{6}\approx2.45$. High temperatures smear out the minimum of N_Σ at $\omega=0$ completely. The solution depicted is stable since at $T=2$ no AB-CDW is possible.

In Fig. 7, stable solutions with $b>0$ are shown. Note the square root divergence in the DOS (left column) in the vicinity of the gap. At $T=0$ the gap is at $2\omega_\Delta\approx0.6$, whereas

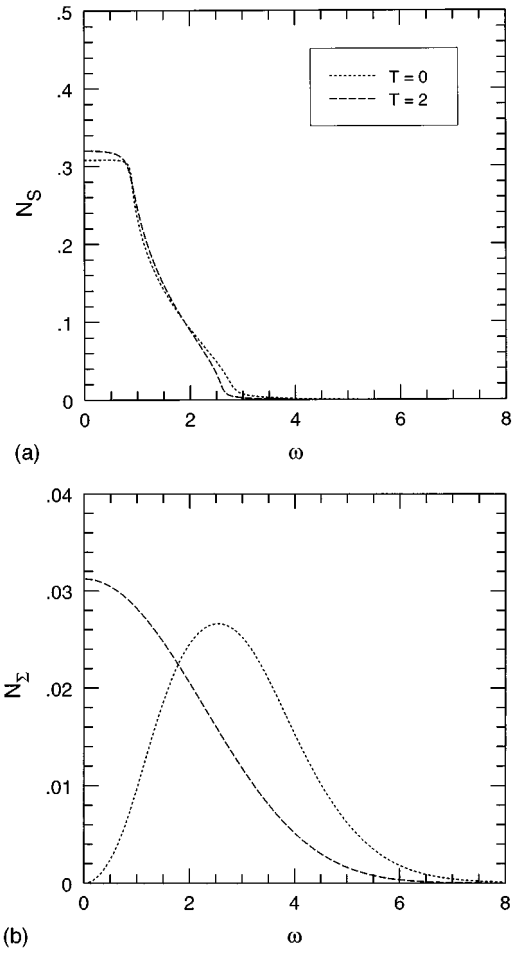

FIG. 6. Density of states and spectral function of the self-energy in the homogeneous phase at $U=2$ and $T=0$ and $T=2$ in $d=3$. For definitions see Eqs. (6).

the spectral density of the self-energy becomes finite at about $1.8\approx6\omega_\Delta$. This results from the two convolutions involved.[6] They cause the gap in the density of the self-energy to be exactly three times the gap in the DOS. Put differently, the finite spectral density of the self-energy corresponds to the inelastic scattering of a particle or a hole involving an additional particle-hole pair. Thus, the necessary minimum energy is three times the elementary gap. The physically important implication is the existence of quasiparticles with energies between ω_Δ and $3\omega_\Delta$ with infinite lifetime. Following the arguments of Luttinger[21] by which he shows that the density of the self-energy generically goes like ω^2 at the Fermi edge one comes to the conclusion that this factor 3 is not an artifact of the approximation but valid to all orders. Therefore, if the conditions are such that the homogeneous phase is a Fermi liquid, i.e., Luttinger's argument holds, a gapped, spontaneously symmetry-broken phase has a factor 3 between the gap in the DOS and the gap in the self-energy. This implies also the existence of undamped quasiparticles which have interesting consequences on the transport properties (see below). The exponent of the power law with which the imaginary parts of the self-energy rise at $\omega=3\omega_\Delta$ is 3/2.

At finite temperatures the energy gap is smaller since the order parameter has decreased. This effect is visible already

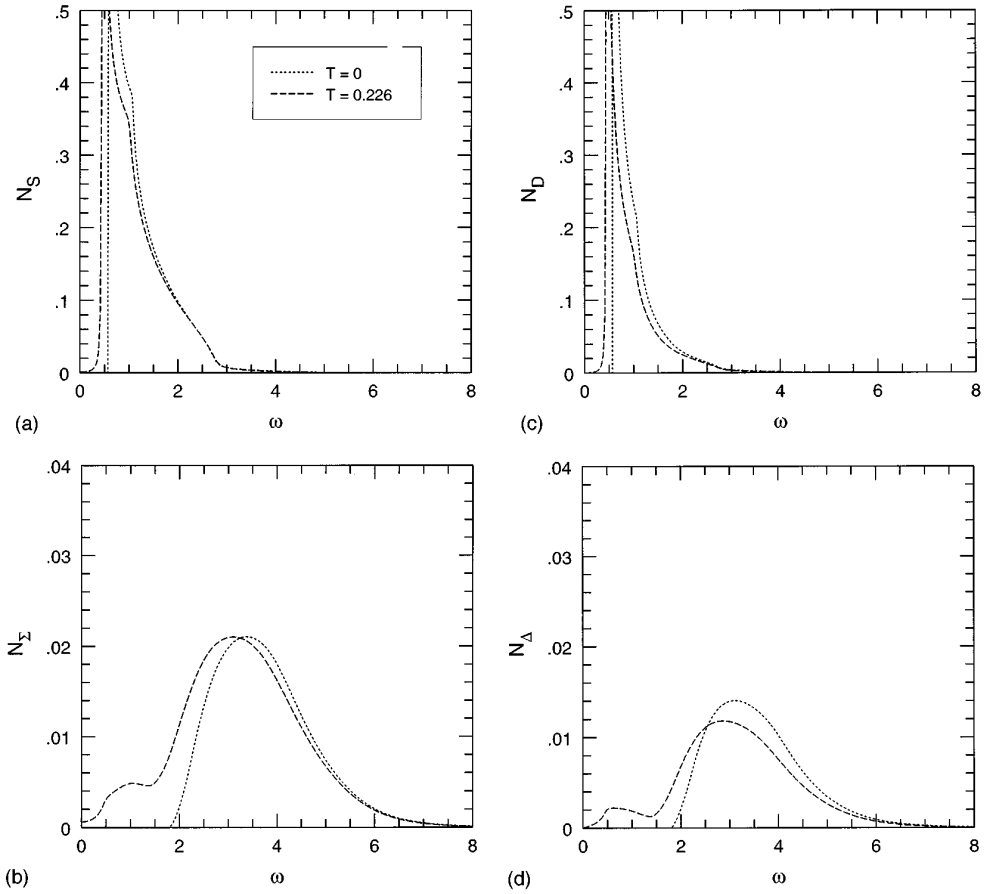

FIG. 7. Density of states and spectral function of the self-energy in the AB charge density wave at $U=2$ and $T=0$ ($b=0.311\,005$), $T=0.225\,658$ ($b=0.250\,000$) in $d=3$. For definitions see Eqs. (6). The sum quantities in (a) and (b) are even functions of frequency; the difference quantities in (c) and (d) are odd functions.

in the Hartree treatment. In addition, the energy gap is smeared out: thermal fluctuations represented by the local correlation term Σ^C induce a certain spectral weight within the ''gap'' which no longer exists in the rigorous sense. The occurrence of two maxima in N_Σ and in N_Δ should be noted.

In Fig. 8, the generic results for large values of the interaction are shown. At $T=0$ the factor 3 between the gap in the DOS and the gap of the spectral densities of the self-energies is even more easily discernible. At the finite temperature ($T\approx 1.5$), all the structures are smeared out; the order parameter is considerably smaller than at $T=0$: $b=0.260$ at finite T to $b=0.479$ at $T=0$. The comparison of the spectral weights of the self-energy at zero and at finite temperature illustrates an important effect. The correlation term is suppressed by the symmetry breaking. The larger b the smaller is the area under the curves in Figs. 8(b) and 8(d). The effect can be understood quantitatively with the help of the equations (18) which imply that the area under the curves vanishes for $b\to 1/2$. This leads to the counterintuitive effect that the significance of the correlation term decreases on increasing interaction at $T=0$ albeit it is quadratic in the interaction

In Fig. 8, hardly discernible satellite bands exist at $\omega\approx 12$. They are engendered by the finite imaginary part of the self-energy at these energies [see Figs. 8(b) and 8(d)]. To demonstrate that there are in fact infinitely many satellite bands with exponentially decreasing weights, the densities N_S and N_Σ are plotted logarithmically in Fig. 9. The principal band of the DOS consists of quasiparticles with infinite life-time at $\omega_\Delta\approx 4$. The satellite bands correspond to peaks in the spectral density of the self-energy. The satellite bands are located at $(2m+1)\omega_\Delta$ where m is an integer. The peaks in the spectral density of the self-energy are located at $(2m+1)\omega_\Delta$ where m is an integer but *not* 0 or -1. This phenomenon is generic for the self-consistent solution of a system of equation comprising convolutions of strongly peaked functions. It appears only at large values of U because it is necessary that $\omega_\Delta\approx U/2$ is larger than the band width in order to resolve the peaks. Note that according to (9), a large value of Δ induces band narrowing. Whereas the principal band is $\sqrt{6}$ wide at $U=0$, its width is shrunk to about unity in Fig. 8(a).

For detailed numerical results on the order parameter as function of interaction and of temperature as well as on the critical temperature the reader is referred to Ref. 6. The asymptotic behavior at small U is discussed analytically by van Dongen.[22,23] In a nutshell, the correlation term renormalizes the Hartree results for b and T_c by a constant factor of order unity which tends to unity for $d\to\infty$.

III. CONDUCTIVITY: FOUNDATIONS

Due to the point symmetry group of the hypercubic lattices the conductivity $\sigma(\omega)$ can be treated as a scalar. Previous one-particle results showed that the treatment on the level of linear $1/d$ corrections should yield reasonable results[6] in $d=3$.

The conductivity is calculated from a two-particle correlation function. This will be done here from the current-current correlation function χ^{JJ}. The conductivity comprises two contributions $\sigma(\omega)=\sigma_1(\omega)+\sigma_2(\omega)$. The first term depends on the occupation of the momentum states $\langle\hat{n}_{\mathbf{k}}\rangle$

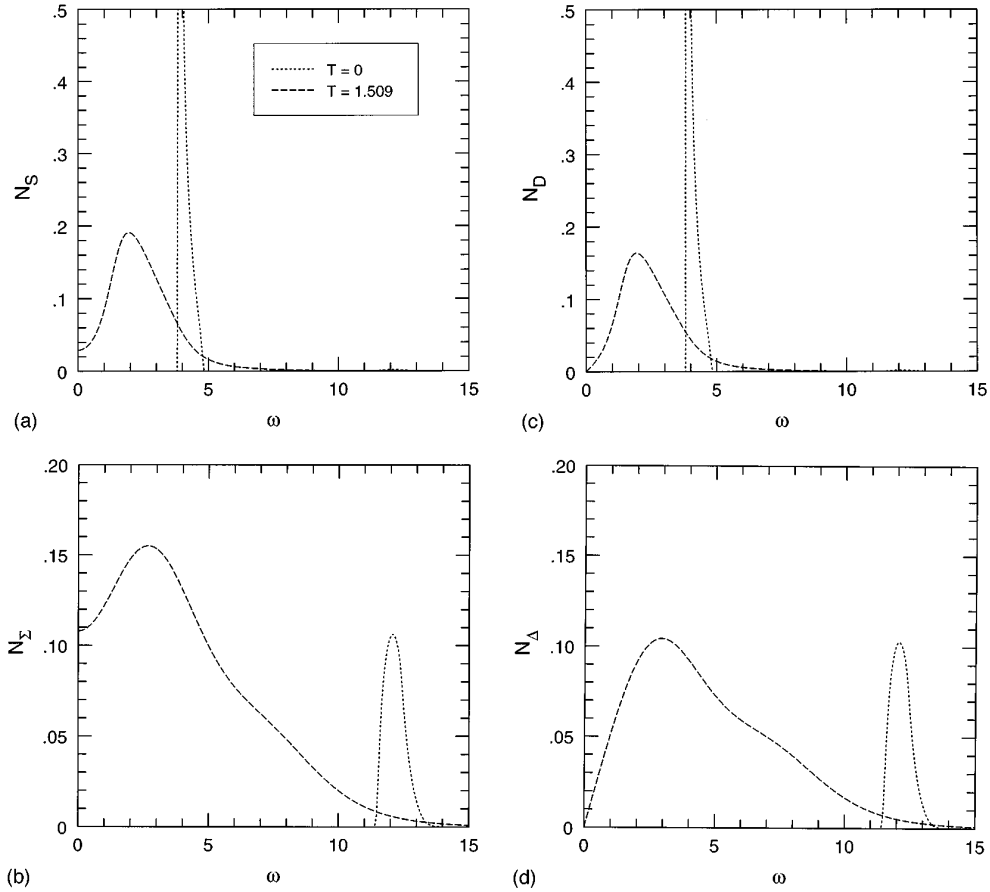

FIG. 8. Density of states and spectral function of the self-energy in the AB charge density wave at $U=8$ and $T=0$ ($b=0.479\,312$), $T=1.509\,384$ ($b=0.260\,004$) in $d=3$. For definitions see Eqs. (6). At $\omega\approx 12.0$ hardly visible satellite bands are present in N_S and N_D for $T=0$. They result from the imaginary parts of the self-energy around this frequency.

whereas the second term is proportional to $\chi^{\mathrm{JJ}}(\omega)$,[24]

$$\sigma_1(\omega)=\frac{i}{\omega}\int_{\mathrm{BZ}}\frac{\partial^2\varepsilon(\mathbf{k})}{\partial k_1^2}\langle\hat{n}_{\mathbf{k}}\rangle\frac{dk^d}{(2\pi)^d}, \tag{20a}$$

$$\sigma_2(\omega)=\frac{i}{\omega}\chi^{\mathrm{JJ}}(\omega). \tag{20b}$$

The current-currrent correlation function will be computed including $1/d$ corrections with the help of the Baym/Kadanoff formalism.[12,13] Specific correlation functions are determined from the general two-particle correlation function $L(12,1'2')$ via

$$\chi^{AB}=\int A(1,1')L(12,1'2')B(2,2')d11'22'. \tag{21}$$

The numbers stand for composite space and time coordinates (or momentum and frequency coordinates). The measure $d11'22'$ tells which coordinates are integrated. The quantities A and B represent the operators for which the correlation function is computed. The Bethe-Salpeter equation determines $L(12,1'2')$ implicitly using the kernel (or effective two-particle interaction) $\Xi(35,46)$ and the Green function $G(1,2)$,

$$L(12,1'2')=G(1,2')G(2,1')+\int G(1,3)G(1',4)\Xi(35,46)L(62,52')d3456. \tag{22}$$

Like the kernel of the Dyson equation, namely, the self-energy, the kernel $\Xi(35,46)$ of the Bethe-Salpeter equation is given as a functional derivative with respect to the Green function,

$$\Xi(35,46)=\frac{\partial\Sigma(3,4)}{\partial G(6,5)}=\frac{\partial^2\Phi}{\partial G(4,3)\partial G(6,5)}. \tag{23}$$

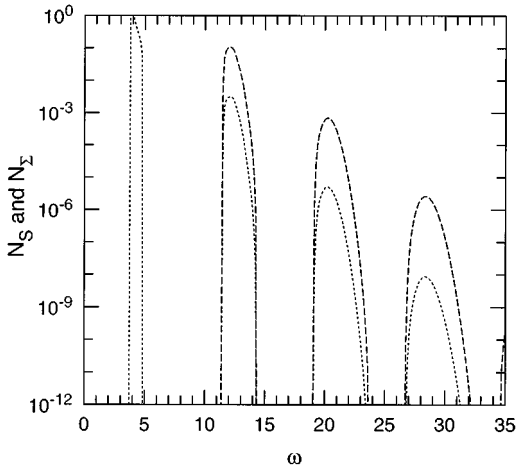

FIG. 9. Density of states N_S (short-dashed curve) and spectral function N_Σ (long-dashed curve) in the AB-CDW at $U=8$ in logarithmic scale. The difference quantities are not shown since their values lie only slightly under those of the sum quantities.

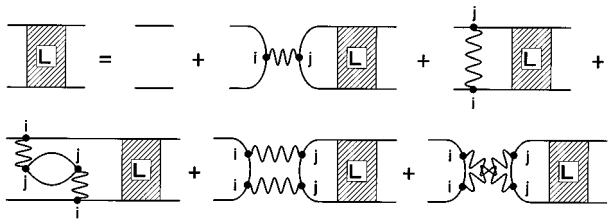

FIG. 10. Diagrammatic representation of the Bethe-Salpeter equation resulting from Φ_A according to Baym/Kadanoff. The wavy lines stand for interaction; the solid ones for fermionic propagators. The direction of the lower propagators is opposite to the one of the upper propagators.

Diagrammatically, the functional derivation is the omission of a propagator line. Applying these steps to the approximate generating functional Φ_A in Fig. 3 yields the diagrammatic representation of the Bethe-Salpeter equation (22) in Fig. 10. The first diagram with a wavy interaction line in the upper row stems from the Hartree diagram, the last diagram in the upper row results from the Fock diagram. The diagrams in the lower row in Fig. 10 are generated by the different possibilities to take out two propagator lines from the correlation diagram.

Fortunately, the summation in Fig. 10 simplifies considerably for the evaluation of the current-current correlation function χ^{JJ}. Figure 11 displays Eq. (21). The squares represent the current vertices

$$J(1,1')=\delta(\mathbf{k}_1-\mathbf{k}_{1'})\,\delta(\omega_1-\omega_{1'}-\omega)\frac{\partial\varepsilon}{\partial k_{1,1}}. \tag{24}$$

Due to symmetry it does not matter for which spatial direction $J(1,1')$ is calculated; $k_{1,1}$ is one arbitrarily chosen component. The crucial property of the current vertex is its oddness as a function of $k_{1,1}$. All interaction terms which are even in $k_{1,1}$ do not contribute. This is the case for all the diagrams resulting from the local correlation in the lower row and for the diagram coming from the Hartree term since only *one* site appears on either side. Hence, only the geometric series depicted in Fig. 12 caused by the nonlocal Fock term is left. For comparison: in the infinite dimensional Hubbard model the simplifications are even more drastic. All vertex corrections drop out and the current-current correlation function is just the convolution of two Green functions.[25]

Let us call the value of the first diagram in Fig. 12 the ''free'' current-current correlation function and let us use the symbol χ_0^{JJ} for it. In the homogeneous phase one obtains with the help of Eqs. (21) and (24) and of the propagator in $\mathbf{k}$ space $[\omega-\Sigma(\omega)-\gamma\varepsilon(\mathbf{k})]^{-1}$

$$\chi_0^{\mathrm{JJ}}(\mathrm{i}\omega_m)=\frac{4T}{Z}\sum_{\omega_\nu-\omega_\lambda=\omega_m}\int_{\mathrm{BZ}}\frac{\sin^2(k_1)}{[w_\nu-\gamma\varepsilon(\mathbf{k})][w_\lambda-\gamma\varepsilon(\mathbf{k})]}\times\frac{dk^d}{(2\pi)^d}, \tag{25}$$

where $w_{\nu/\lambda}:=i\omega_{\nu/\lambda}-\Sigma(i\omega_{\nu/\lambda})$.

We focus now on the segments between two wavy lines in Fig. 12. The conservation of energy and of momentum makes it possible to carry out the sum over all momenta and

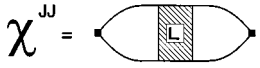

FIG. 11. Diagrammatic representation of Eq. (21) for the current-currrent correlation function.

energies by considering independent momenta and energies circulating in each segment. Then the momentum *in* a wavy line is the difference of two adjacent wave vectors $\mathbf{k}$ and $\mathbf{k}'$. A second time, the evenness and the oddness in the components of the wave vector are used to write for the factor of an interaction line

$$-\frac{U}{d}\sum_{i=1}^{d}\cos(k_i-k_i')=-\frac{2U}{Z}\sum_{i=1}^{d}[\sin(k_i)\sin(k_i')+\cos(k_i)\cos(k_i')]\rightarrow-\frac{2U}{Z}\sin(k_1)\sin(k_1'). \tag{26}$$

The argument is obvious for one of the border segments and follows for those in the middle by induction.

At the end one realizes that each segment corresponds to a factor of $-(U/2)\chi_0^{\mathrm{JJ}}$ which justifies calling the right side of Fig. 12 a geometric series which takes the value

$$\chi^{\mathrm{JJ}}(\omega+0i)=\frac{\chi_0^{\mathrm{JJ}}(\omega+0i)}{1+U\chi_0^{\mathrm{JJ}}(\omega+0i)/2} \tag{27}$$

after analytic continuation. The derivation of a similar formula in the AB-CDW is given in Appendix B. The results are cited below.

The momentum integration in Eq. (25) requires a modified DOS, to be called the conductivity DOS henceforth,

$$N_{c,0}(\omega):=\int_{\mathrm{BZ}}\sin^2(k_1)\,\delta(\omega-\varepsilon(\mathbf{k}))\frac{dk^d}{(2\pi)^d}, \tag{28}$$

from which we define also the conductivity Green function $g_{c,0}(z):=\int_{-\infty}^{\infty}N_{c,0}(\omega)/(z-\omega)d\omega$. The conductivity DOS can be simply derived once the DOS is known. These two functions are related via

$$N_0(\omega)=-\frac{2}{\omega}\frac{\partial N_{c,0}}{\partial\omega}(\omega). \tag{29}$$

This relation stems from the fact that one has to replace one of the d factors $(1/\pi)1/\sqrt{t^2-\omega^2}$ in the convolution for the DOS by $(1/\pi)\sqrt{t^2-\omega^2}$ in order to calculate the conductivity DOS. The derivation uses the representation of convolutions as products in Fourier space.

FIG. 12. Current-currrent correlation function with $1/d$ corrections.

Using the definition of the conductivity Green function and partial fraction expansion it is straightforward to rewrite Eq. (25) as

$$\chi_0^{\mathrm{JJ}}(\mathrm{i}\omega_m) = -\frac{4T}{\gamma Z}\sum_{\omega_\nu-\omega_\lambda=\omega_m}\frac{g_c(i\omega_\nu/\gamma)-g_c(i\omega_\lambda/\gamma)}{w_\nu-w_\lambda}. \tag{30}$$

Analytic continuation of the latter gives the general formula [Eq. (14) in Ref. 26] for the current-current correlation function in the homogeneous phase.

In the AB-CDW, it is also possible to sum the series in Fig. 12 as geometric series. The main difference is the fact that 2×2 matrices instead of scalars are involved. The details are given in Appendix B; the results[27] are

$$\chi^{\mathrm{JJ}}(i\omega_m)=\frac{2}{U}-\frac{2}{U}\frac{1-A_2}{(1-A_1)(1-A_2)-A_3^2}, \tag{31}$$

where the quantities A_1,A_2, and A_3 are defined by

$$A_1(i\omega_m)=\frac{2UT}{Z}\sum_{\omega_\nu-\omega_\lambda=\omega_m}\left[\frac{(w_\lambda+w_\nu)[g_{c,S}(i\omega_\nu)-g_{c,S}(i\omega_\lambda)]-[\Delta(i\omega_\lambda)+\Delta(i\omega_\nu)][g_{c,D}(i\omega_\nu)-g_{c,D}(i\omega_\lambda)]}{w_\nu^2-w_\lambda^2-[\Delta^2(i\omega_\nu)-\Delta^2(i\omega_\lambda)]}\right], \tag{32a}$$

$$A_2(i\omega_m)=\frac{2UT}{Z}\sum_{\omega_\nu-\omega_\lambda=\omega_m}\left[\frac{(w_\lambda-w_\nu)[g_{c,S}(i\omega_\nu)+g_{c,S}(i\omega_\lambda)]-[\Delta(i\omega_\lambda)-\Delta(i\omega_\nu)][g_{c,D}(i\omega_\nu)+g_{c,D}(i\omega_\lambda)]}{w_\nu^2-w_\lambda^2-[\Delta^2(i\omega_\nu)-\Delta^2(i\omega_\lambda)]}\right], \tag{32b}$$

$$A_3(i\omega_m)=\frac{2UT}{Z}\sum_{\omega_\nu-\omega_\lambda=\omega_m}\left[\frac{\Delta(i\omega_\lambda)g_{c,S}(i\omega_\nu)-w_\lambda g_{c,D}(i\omega_\nu)+\Delta(i\omega_\nu)g_{c,S}(i\omega_\lambda)-w_\nu g_{c,D}(i\omega_\lambda)}{w_\nu^2-w_\lambda^2-[\Delta^2(i\omega_\nu)-\Delta^2(i\omega_\lambda)]}\right]. \tag{32c}$$

In complete analogy to the usual Green functions, the conductivity Green functions are $g_{c,S}:=(g_{c,A}+g_{c,B})/2$ and $g_{c,D}:=(g_{c,A}-g_{c,B})/2$, hence

$$g_{c,S}(\omega)=\frac{\omega-\Sigma(\omega)}{\gamma\sqrt{[\omega-\Sigma(\omega)]^2-\Delta^2(\omega)}}g_{c,0}(\sqrt{w^2-\Delta^2(\omega)}/\gamma), \tag{33a}$$

$$g_{c,D}(\omega)=\frac{\Delta(\omega)}{\gamma\sqrt{w^2-\Delta^2(\omega)}}g_{c,0}(\sqrt{w^2-\Delta^2(\omega)}/\gamma), \tag{33b}$$

which compares to Eq. (9) [w is shorthand for $\omega-\Sigma(\omega)$].

Now a relation for the dc conductivity shall be derived. In order that the limit $\lim_{\omega\to 0}\sigma(\omega)$ exists,

$$\chi^{\mathrm{JJ}}(0)=\int_{\mathrm{BZ}}\frac{\partial^2\varepsilon}{\partial k_1^2}(\mathbf{k})\langle\hat{n}_{\mathbf{k}}\rangle\frac{dk^d}{(2\pi)^d}=\frac{\langle\hat{T}\rangle}{d} \tag{34}$$

must hold according to Eq. (20). The operator $\hat{T}$ stands for the kinetic energy. Equation (34) implies also the f sum rule $\int_{-\infty}^{\infty}(i\chi^{\mathrm{JJ}}/\omega)d\omega=-\pi\langle\hat{T}\rangle/d$. At the end of Appendix B, it is shown explicitly that Eq. (34) is valid since A_3 vanishes at $\omega=0$ and $A_1=-U\langle\hat{T}\rangle/(2\gamma d)=1-1/\gamma$. For the dc conductivity one obtains

$$\sigma(0)=i\left.\frac{\partial\chi^{\mathrm{JJ}}}{\partial\omega}\right|_{\omega=0}=-\left.\frac{2i\gamma^2}{U}\frac{\partial A_1}{\partial\omega}\right|_{\omega=0}. \tag{35}$$

For explicit evaluation it is useful to split $\sigma_{\mathrm{dc}}(0)$ into a term including retarded and advanced Green functions σ_{dc1} and a term including only retarded or advanced Green functions σ_{dc2} after analytic continuation. This yields

$$\sigma_{\mathrm{dc1}}=\frac{\gamma^2}{\pi Z}\int_{-\infty}^{\infty}\frac{(1-\mathrm{Re}\Sigma)N_{c,S}-(\mathrm{Re}\Delta)N_{c,D}}{(1-\mathrm{Re}\Sigma)N_\Sigma+(\mathrm{Re}\Delta)N_\Delta}(-f_F'(\omega))d\omega, \tag{36}$$

where $f_F'(\omega)$ is the derivative of the Fermi distribution, and

$$\begin{aligned}\sigma_{\mathrm{dc2}}=&-\frac{\gamma^2}{\pi Z}\int_{-\infty}^{\infty}\left.\frac{(1-\Sigma)\partial_\omega g_{c,S}-\Delta\partial_\omega g_{c,D}}{(1-\Sigma)(\partial_\omega\Sigma-1)+\Delta\partial_\omega\Delta}\right|_{\omega+0i}\\&\times(-f_F'(\omega))d\omega\\=&\frac{1}{\pi Z}\Bigg[1-\mathrm{Re}\int_{-\infty}^{\infty}[(\omega-\Sigma)g_S-\Delta g_D]_{\omega+0i}\\&\times(-f_F'(\omega))d\omega\Bigg].\end{aligned} \tag{37}$$

In the last expressions, all the Green functions are retarded. In the homogeneous phase, the contribution (36) is more important than the one in Eq. (37). The former diverges for $T\to 0$ and $\omega\to 0$, the latter does not. In the symmetry broken AB-CDW, however, both terms turn out to be essential.

Equations (31), (32), (36), and (37) are the foundation for the calculation of the conductivity for zero and for nonzero order parameter. The focus of the present work is on the AB-CDW. The properties of the conductivity in the homogeneous phase (e.g., Fermi liquid behavior) are presented in detail in Ref. 26, where also the influence of the truncation of the $1/d$ expansion is discussed.

IV. CONDUCTIVITY: RESULTS

In this section we present and discuss results which follow from the general equations derived in the preceding section. All results are calculated at half-filling and for $d=3$.

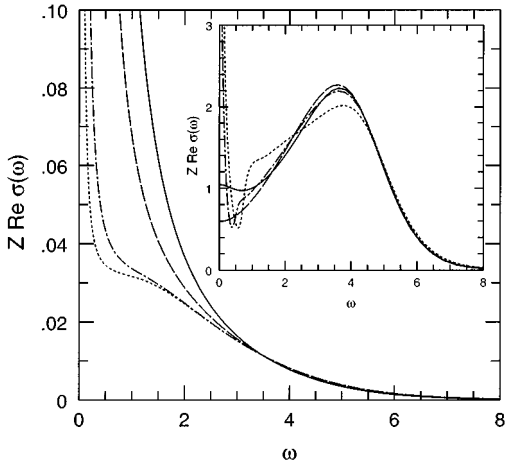

FIG. 13. Scaled real part of the dynamic conductivity $\mathrm{Re}\sigma(\omega)$ in the nonsymmetry broken phase at $U=4.243$ for $T=0.393$ (solid lines), $T=0.196$ (dashed lines), $T=0.049$ (dashed-dotted lines), and $T=0.025$ (dotted lines). Main figure, spinless fermions in $d=3$; inset, Hubbard model in the noncrossing approximation (data from Pruschke).

In Fig. 13, the real part of the dynamic conductivity is depicted in the nonsymmetry-broken phase for different temperatures, i.e., the occurrence of a symmetry-broken phase at low temperature is discarded deliberately for the moment. They are compared with results of Pruschke, Cox, and Jarrell[28,29] for the half-filled Hubbard model in $d=\infty$, obtained in the noncrossing approximation. In both cases the interaction value is $U=4.243$ (in our units) which is just below the value where the Mott-Hubbard transition occurs in the Hubbard model.[29] For spinless fermions the Drude peak is absolutely dominant. Its weight is very large. Its width is given by the imaginary part of the self-energy at the Fermi level $N_\Sigma(0)$ [see Eq. (32) with $\Delta=0$ or Eq. (14) in Ref. 26], i.e., the width is proportional to T^2. The shape of the Drude peak corresponds very well to a Lorentzian.

Only at low temperatures does a shoulder emerge. This shoulder is the effect of interaction induced scattering. The fluctuations are not particularly strong. It was already shown previously[26] that the average over the Z interaction partners reduces the relative fluctuations. There is no Mott-Hubbard transition without symmetry breaking in the spinless fermion model because an increasing interaction enhances not only the fluctuations but also the Fock term (absent in the Hubbard model) which stabilizes the Fermi liquid phase. These features are particularly obvious in the comparison with the Hubbard model data. In this model, the Drude peak is very reduced at all displayed temperatures since much of the weight is shifted to the peaks induced by the strong local particle density fluctuations.

Besides the difference shoulder vs peak it is interesting to note the difference in energy scales. In the Hubbard model, it is more or less U which sets the energy at which the peak occurs. This can be understood as the energetic effect of whether or not an electron with a different spin is present. The typical energy for the shoulder is obviously much smaller. This in turn can be understood in the same way as before but it has to be taken into account that the number of possible interaction partners Z leads to a reduction of the relative fluctuations of the order of $1/\sqrt{Z}$. This yields an energy of roughly 1.7 in the particular example which is in good agreement with the numerical result.

Due to the nesting at half-filling, the system of spinless fermions undergoes a transition to a spontaneously broken translation symmetry for all (positive) values of the interaction on lowering the temperature. This spontaneously broken discrete symmetry implies the occurrence of a gap which grows exponentially $\omega_\Delta \propto \exp(-c/U)$ for low values of the interaction at $T=0$ (see Ref. 6 and references therein). It is visible in the dynamic conductivity.[27] In Fig. 14, its growth on decreasing temperature is shown in four snapshots. In Fig. 14(a), T is still above its critical value. No structure is visible except for the dominant Drude peak already discussed in Fig. 13. In Figs. 14(b)–14(d) the gap is present and discernible. Its value is approximately $2\omega_\Delta$ if ω_Δ is the value of the energy gap in the DOS, see Figs. 7 and 8. But there is also some weight within the gap for $T>0$ since the correlation contribution blurred already the gap in the DOS. Note in passing that the f sum rule can be verified numerically on the results shown in Fig. 14 very accurately (to the fraction of a percent at $T=0$; to the fraction of a permille in the homogeneous phase).

The Drude peak does not vanish immediately in the AB-CDW. It becomes smaller and narrower on decreasing temperature. Its maximum value does not vanish for $T\to 0$ (see below) but its weight does. In Fig. 15, two frequency intervals are shown in detail for a fairly low temperature. Figure 15(a) displays the Drude peak again. The interesting feature is its small width [compared with the width of the Drude peaks in Figs. 14(b) and 14(c)]. It cannot be explained by a factor of T^2 but corresponds to an exponential shrinking $\exp(-\omega_\Delta/T)$. As already observed in the one-particle properties, an increasing gap reduces the influence of the fluctuations.

Figure 15(b) shows a very interesting feature below the proper band edge at $\omega\approx 2\omega_\Delta$. This resonance is also visible in Fig. 14(c) whereas the resonance and the band edge are not resolved at a higher temperature, Fig. 14(b). The resonance can be approximated very well by a Lorenztian. At $T=0$, it is also present as a δ peak [not shown in Fig. 14(d)]. It originates from a zero of the denominator in Eq. (31). At $T>0$, only the real part of the denominator vanishes and its imaginary part leads to the observed broadening which depends strongly, namely exponentially, on the temperature.

Physically the resonance can be interpreted as a bound state, an exciton, between a particle in the upper band and a hole in the lower band in the reduced Brillouin zone of the AB-CDW. The energy difference between the position of the exciton and the band edge is its binding energy. The type of diagrams which yield the denominator in Eq. (31) corroborates the interpretation as an exciton. The vertical interaction lines stand for the repeated interaction between particle and hole in the two propagators involved in the calculation of χ^{JJ}. It should be noted that, for instance, for the parameters of Fig. 14(d) about 70% of the weight of the conductivity is found in the excitonic resonance (one may not be misled by the logarithmic scale). This means that the excitonic effect is not at all a small side effect.

Concluding the part on the dynamic conductivity, we dis-

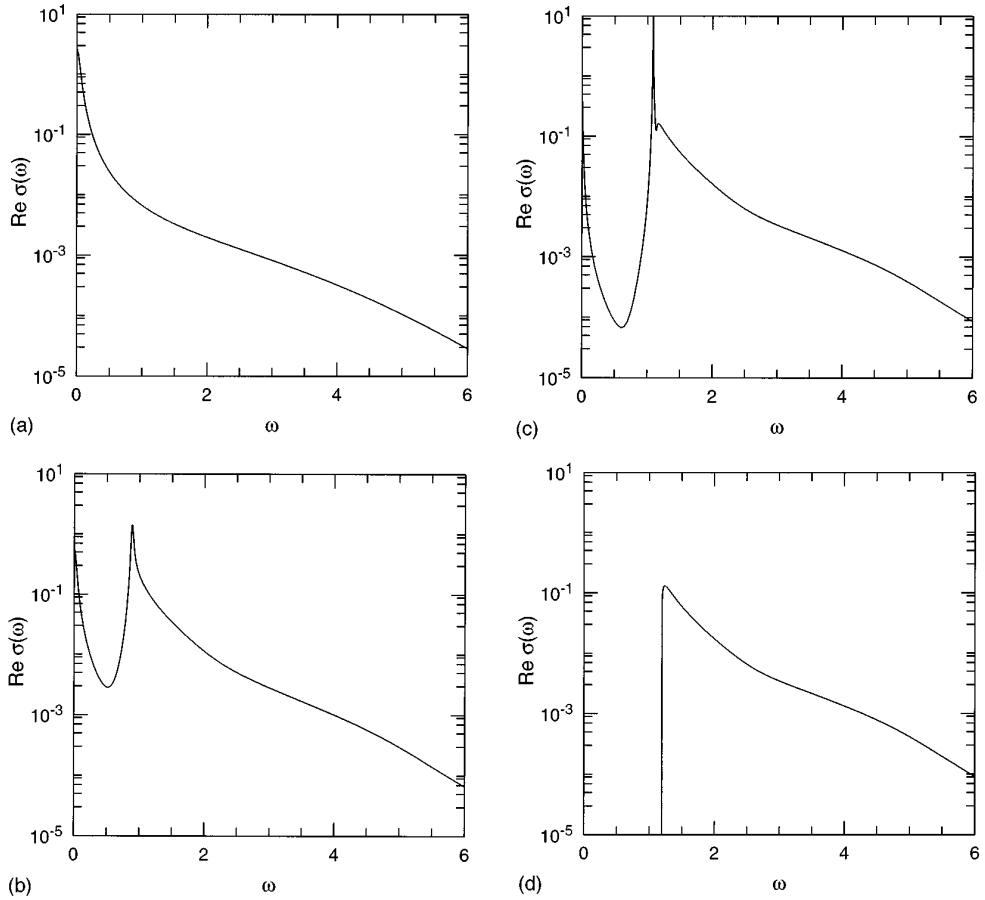

FIG. 14. Real part of the dynamic conductivity $\mathrm{Re}\sigma(\omega)$ in $d=3$ at $U=2.0$ in logarithmic scale. (a) $T=0.300\,000$ and $b=0$; (b) $T=0.225\,658$ and $b=0.250\,000$; (c) $T=0.155\,286$ and $b=0.299\,801$; (d) $T=0$ and $b=0.311\,005$. In (d) the δ peak at $\omega=1.133\,12$ is not shown, its weight is 0.062 336.

cuss Fig. 16, which shows results for a large interaction value U. Due to the induced large gap and due to the narrow effective bandwidth, several frequency intervals of absorption are well separated. The peaks are caused by the convolution of the satellite band presented for the one-particle properties. Note, however, that the weight of these satellites decreases rapidly by a factor of 100 from peak to peak. These small amplitudes render an experimental verification certainly extremely difficult if not impossible. Nevertheless, it would be interesting to know whether such satellites exist. Their existence would support the application of a self-consistent approximation since the non-self-consistent calculation yields only two peaks besides the δ peak which is not shown.

Since the dc conductivity in the absence of symmetry breaking has been extensively discussed in Ref. 26, we will treat here exclusively the case with symmetry breaking. The result of Eqs. (36) and (37) is depicted in Fig. 17 for weak and strong interaction.[27] To the right of the cusp the system is in the nonsymmetry-broken phase. The conductivity is essentially proportional[26] to T^2. On entering the symmetry-broken phase with gap, the conductivity falls drastically since the energy gap reduces the DOS at the Fermi level. Surprisingly, however, the conductivity does *not* vanish for $T\rightarrow 0$ although the DOS vanishes in this limit. There is even a very slight uprise of σ_{dc} close to $T=0$. This phenomenon is again a manifestation of the suppression of correlation effects by the energy gap. The DOS is reduced by a factor of $\exp(-\omega_\Delta/T)$, but so is the imaginary part of the self-energy in Eq. (32) which is responsible for the quasiparticle lifetime. These two effects cancel exactly. Put differently, an exponentially small number of quasiparticles of exponentially large lifetime carries a constant current (but see Discussion below). It remains an algebraic dependence on T of the dc conductivity. The constant term and the linear one can be computed analytically and were used to complete the curves in Fig. 17 for small values of T where the numerical calculation is no longer precise enough due to extinction.

The limit value $\lim_{T\rightarrow 0}\sigma(\omega=0)$ is given in Fig. 18 as a function of U. As expected, it decreases rapidly for $U\rightarrow\infty$. Note the logarithmic scale.

What do the above findings for σ_{dc} imply for the existence of a metal-insulator transition? Seemingly, even spontaneous symmetry breaking does not suffice to render the system insulating. But it must be noted that the ''residual'' conductivity $\lim_{T\rightarrow 0}\sigma(\omega=0)$ is infinitely fragile: any other arbitrarily weak scattering mechanism which does not die out on $T\rightarrow 0$, e.g., disorder or scattering at the borders of the sample, will take over. The exponentially vanishing DOS will yield an exponentially vanishing dc conductivity. This is reflected in the exponentially decreasing width of the Drude peak, which, at constant height, implies an exponentially decreasing weight.

Experimentally, very pure samples might allow us to see the beginning of the plateaus in Fig. 17 before the above-cited other scattering mechanism reduces the conductivity. This behavior is in complete analogy to the one observed for the shear viscosity $\eta(T)$ of helium 3 in the B phase.[30]. In this system, as in the system of spinless fermions in the AB-CDW, one observes an exponentially diverging mean free

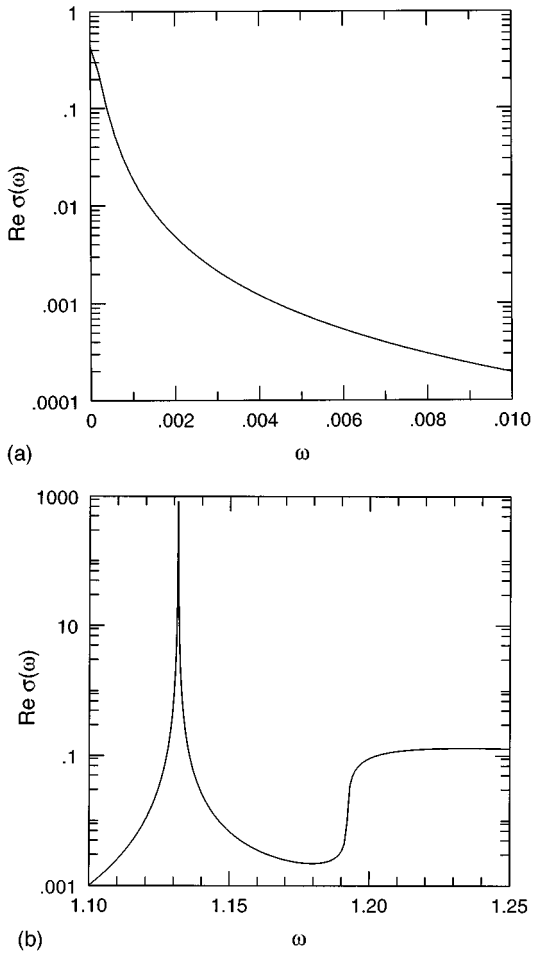

FIG. 15. Enlargements of two frequency intervals for $T=0.083\,383\,3$ and $b=0.310\,773$. (a) shows details of the Drude peak; (b) the excitonic resonance.

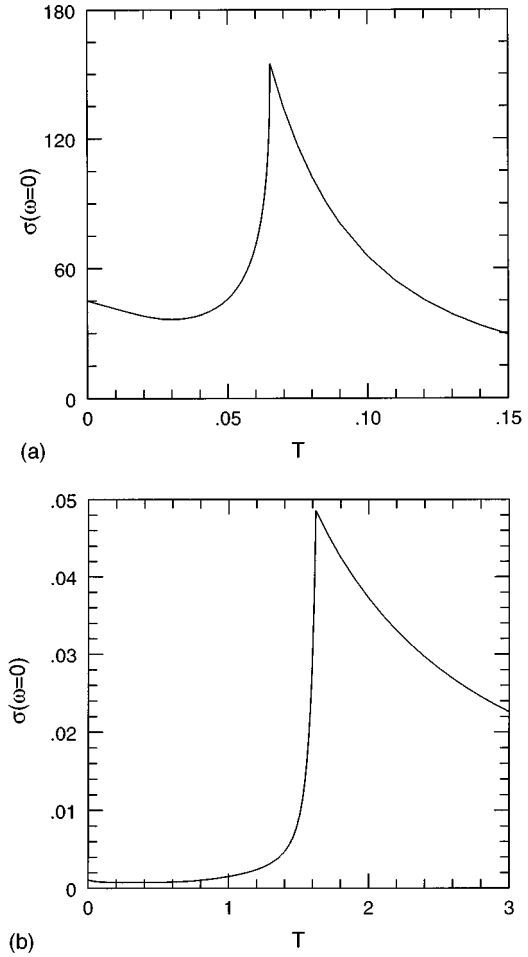

FIG. 17. Temperature dependence of the dc conductivity at $U=1.0$ (a) and at $U=8.0$ (b). Below $T=0.026$ in (a) and below $T=0.6$ in (b) a fit was used (see main text).

path since the collision between (quasi)particles is suppressed by a gap. In the so-called ''Knudsen regime'' collisions of quasiparticles with the wall of the container dominate the collisions *between* the quasiparticles. In helium 3, one observes a sharp drop below T_c and then the beginning of a plateau before finally $\eta(T)$ vanishes rapidly. The theoretical result for the infinite system predicts a gentle uprise just like the one we predict in Fig. 17. In both cases, a factor $\exp(-\omega_\Delta/T)$ in the DOS cancels with the same factor in the

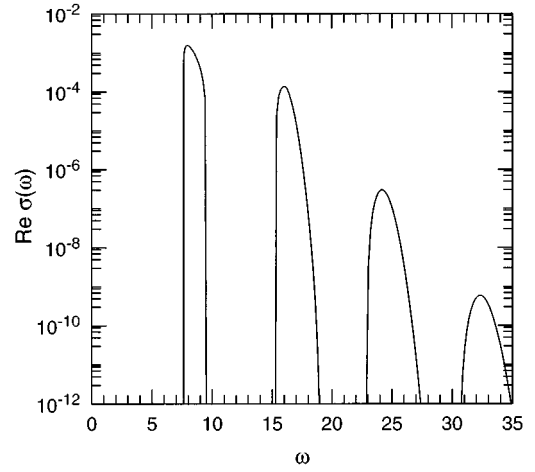

FIG. 16. Real part of the dynamic conductivity $\mathrm{Re}\sigma(\omega)$ in $d=3$ at $U=8.0$ for $T=0$ in logarithmic scale. The δ distribution is not displayed.

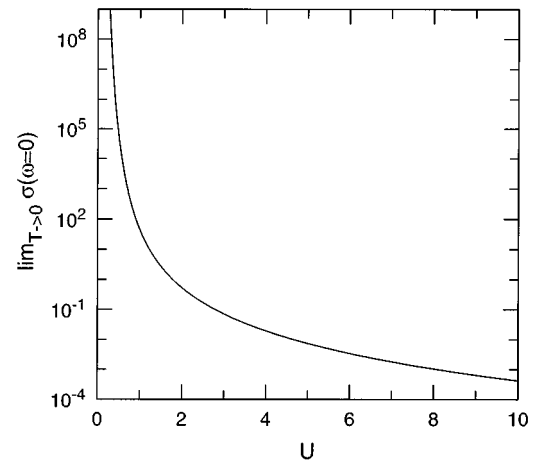

FIG. 18. dc conductivity $\sigma(\omega=0)$ in the limit $T\to 0$ in logarithmic scale.

scattering rate.[30] This interesting analogy underlines the validity of the results of our $1/d$ approach.

V. DISCUSSION

Two main questions are addressed in the present paper: (i) How can an infinite dimensional result be improved by including $1/d$ corrections in a systematic way? (ii) Which influence does spontaneous symmetry breaking have on the conductivity?

It turned out that it is highly nontrivial to construct systematic and reasonable approximations to arbitrary order. This is true already on the conceptual level. It was argued in detail that the self-consistent calculation has certain advantages since it yields thermodynamically consistent and conserving approximations. The Baym/Kadanoff formalism, however, is *not sufficient* to guarantee an approximation which is free from obvious contradictions. It was shown that an inappropriate approximation may lead to the wrong analytic behavior of Green functions and self-energies even though the approximation was derived from a generating functional.

A general theorem was presented which allows us to judge whether wrong analyticity may occur. If the conditions of the theorem are fulfilled, the appearance of the wrong analyticity is excluded. This theorem explains a couple of observations that were made in recent years on the application of perturbation expansions and/or $1/d$ expansions. It is used to show that the self-consistent treatment of $1/d$ corrections for spinless fermions is a good approximation: it possesses the necessary analytic behavior.

For $1/d$ corrections in the Hubbard model the presented theorem makes no statement since the self-energy already has an imaginary part for $d=\infty$. This does not imply that the systematic inclusion of $1/d$ corrections for the Hubbard model is impossible, but one may expect further difficulties. As a matter of fact, analyticity problems have been encountered in the first calculations of $1/d$ corrections in the Hubbard model.[3]

It should be stated that the self-consistent treatment of $1/d$ corrections to any finite order in $1/d$ remains a mean-field theory. As in the $d=\infty$ treatment of the Hubbard model,[9] the mean field is dynamic, i.e., it retains a dependence on frequency. But in the skeleton diagrams, which are considered in any finite order in $1/d$, only lattice sites of *finite* distance occur. This means that critical fluctuations are always cut off. In $d=1$, for instance, the inclusion of $1/d$ corrections reduces the order parameter considerably[6] but does not destroy the order completely.

In the self-consistent $1/d$ treatment of spinless fermions, two-particle properties can be reached, too. In this work, the Bethe-Salpeter equation was set up in general and solved in the particular case of the conductivity $\sigma(\omega)$. This was possible for the nonsymmetry-broken phase as well as for the charge density wave. The equations were evaluated in $d=3$ since the approximation should yield the best results for this value of all experimentally accessible dimensions.[6]

A number of phenomena were described in the $1/d$ expansion which can be compared with other theoretical predictions or experiments.

(i) The dynamic conductivity $\sigma(\omega)$ in the homogeneous phase has a Drude peak. Its width decreases quadratically in T for small values of T. The dc conductivity is always finite.[26]

(ii) The Drude peak persists in the CDW but its weight vanishes exponentially $\propto\exp(-\omega_\Delta/T)$, where ω_Δ is the gap in the one-particle spectra. The height of the Drude peak, however, does *not* vanish since the diverging quasiparticle lifetime cancels the vanishing density of states.

(iii) The real part of $\sigma(\omega)$ displays a band edge at $\approx 2\omega_\Delta$. The singularity at the edge is a square root. Just below the edge an excitonic resonance is situated which is the bound state between a particle and a hole in the empty and in the full band, respectively. These bands are created by the spontaneous symmetry breaking.

(iv) For strong interactions the real part of $\sigma(\omega)$ shows exponentially decreasing peaks at $\omega\approx 2m\omega_\Delta; m\in\{1,2,3,\ldots\}$, which reflect the peaks in the one-particle DOS at $\omega\approx(2m-1)\omega_\Delta$.

(v) Strictly speaking, there is no metal-insulator transition. But the Drude weight decays rapidly on $T\to 0$. Finally, other scattering mechanisms will dominate over quasiparticle-quasiparticle collisions.

In summary, we conclude that the self-consistent treatment of $1/d$ corrections describes successfully a large variety of phenomena since it includes the leading frequency dependence of the self-energy. It is a generalized and improved mean-field theory.

ACKNOWLEDGMENTS

The author is grateful to D. Vollhardt and E. Müller-Hartmann for valuable hints and to Th. Pruschke for the data shown in the inset of Fig. 13. The author would like to thank H. J. Schulz, V. Janiš, P. G. J. van Dongen, and R. Vlaming for helpful discussions and the Laboratoire de Physique des Solides for its hospitality. Furthermore, the author acknowledges the financial support of the Deutsche Forschungsgemeinschaft (SFB 341 and individual grant) and of the European Community (Grant ERBCHRXCT 940438).

APPENDIX A: GENERAL DERIVATION OF THE THEOREM

Let us consider a general correlated fermion problem without magnetic field. A one-particle basis $\{b_i^+\}$ (b_i^+ fermionic creation operator) can be chosen in which the free (one-particle) Hamiltonian can be represented as a real matrix $\mathbf{h}^{(0)}$. The retarded self-energy and the retarded full (interacting) Green function are matrices as well. They might be complex. The argument runs at an arbitrary but fixed value of ω. According to the Dyson equation one has

$$\mathbf{G}=(\omega+0i-\mathbf{h}^{(0)}-\mathbf{\Sigma})^{-1}. \tag{A1}$$

The full Green function can be written as $\mathbf{G}=\mathrm{Re}\mathbf{G}+i\mathrm{Im}\mathbf{G}$, where the real and the imaginary parts are real, symmetric matrices. The same is true for the self-energy. Let us define in particular $\mathbf{B}:=-\mathrm{Im}\mathbf{\Sigma}$.

The aim is to show (a) that the leading order $\mathbf{B}^{(m)}$ in λ of the matrix $\mathbf{B}$ is positive semidefinite and (b) that this implies

that all spectral densities are non-negative. The main difference to the argument in the main part is that the matrices do not commute in general.

All one-particle Green functions $-\langle \mathcal{T}\{a(t)a^+(0)\}\rangle$ have positive spectral densities.[10] Here $\mathcal{T}$ is the time-ordering operator and a^+ (a) is an arbitrary fermionic creation (annihilation) operator. Hence, one has for the corresponding vector $\mathbf{v}$ defined by $a^+ =: \Sigma_i v_i b_i^+$

$$0 \leqslant \mathbf{v}^+ (\mathrm{Im}\mathbf{G})\mathbf{v}. \tag{A2}$$

Since the above equation holds for any $\mathbf{v}$, it implies that the imaginary part of $\mathbf{G}$ is negative semidefinite. Expanding Eq. (38) in powers of $\mathbf{B}$ and resumming the imaginary part yields

$$\mathrm{Im}\mathbf{G} = -\mathbf{A}^{-1}\mathbf{B}\mathbf{A}^{-1}(1+\mathbf{B}\mathbf{A}^{-1}\mathbf{B}\mathbf{A}^{-1}), \tag{A3}$$

where $\mathbf{A} := \omega - \mathbf{h}^{(0)} - \mathrm{Re}\,\mathbf{\Sigma}$. In leading order in λ this becomes

$$\mathrm{Im}\mathbf{G} = -\lambda^m(\omega-\mathbf{h}^{(0)})\mathbf{B}^{(m)}(\omega-\mathbf{h}^{(0)}) + \mathcal{O}(\lambda^{(m+1)}). \tag{A4}$$

The negative semidefiniteness of the lhs of Eq. (A4) implies the positive semidefiniteness of $\mathbf{B}$ for values of ω which are no eigenvalues of $\mathbf{h}^{(0)}$. Assuming continuity[31] for $\mathbf{B}^{(m)}(\omega)$ the positive semidefiniteness extends to all frequencies.

Addressing the sign of the imaginary part of the full Green function we state that $\mathbf{B} \geqslant 0$ implies that there is a matrix $\sqrt{\mathbf{B}}$ which is real and symmetric as well. Defining $\mathbf{D} := \sqrt{\mathbf{B}}\mathbf{A}^{-1}\sqrt{\mathbf{B}}$ allows Eq. (A3) to be written as

$$\mathrm{Im}\mathbf{G} = -\mathbf{A}^{-1}\sqrt{\mathbf{B}}(1+\mathbf{D}^2)^{-1}\sqrt{\mathbf{B}}\mathbf{A}^{-1}. \tag{A5}$$

The expression in parentheses is manifestly positive semidefinite, thus its inverse as well. Since $\mathbf{A}^{-1}\sqrt{\mathbf{B}}$ and $\sqrt{\mathbf{B}}\mathbf{A}^{-1}$ are transposed, the rhs in Eq. (A5) is negative semidefinite as a whole. This concludes the argument.

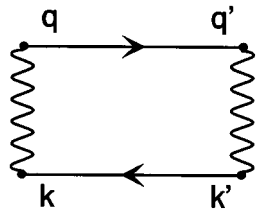

FIG. 19. Diagrammatic basis element of the terms in the sum in Fig. 12

APPENDIX B: CONDUCTIVITY IN THE AB-CDW

In this appendix the geometric series of Fig. 12 is derived in the case of finite order parameter. Furthermore the derivation of Eq. (34) is given.

In the AB-CDW the propagators are not diagonal in $\mathbf{k}$ space. There is the possibility of a transition $\mathbf{k} \to \mathbf{k}+\mathbf{Q}$. The matrix element for this process is the off-diagonal element in Eq. (8). If the wave vector remains unchanged the diagonal matrix elements have to be used. Let us classify the segments between two adjacent wavy lines in a diagram in Fig. 12. A generic segment is shown in Fig. 19. Note that the momentum of the upper propagator cancels the momentum in the lower propagator up to multiples of $\mathbf{Q} = (\pi,\pi,\pi)^\dagger$, since we are interested in the average conductivity. At the end-vertices no momentum is added or subtracted. The case $\mathbf{k}=\mathbf{k}'=\mathbf{q}=\mathbf{q}'$ can be combined with the case $\mathbf{k}=\mathbf{q}=\mathbf{k}'+\mathbf{Q}=\mathbf{q}'+\mathbf{Q}$. In both cases the momentum through the whole segment is zero. Using the elements from Eq. (8) one obtains

$$A_1 = -\frac{2UT}{Z}\sum_{\omega_\nu-\omega_\lambda=\omega_m}\int_{-\infty}^{\infty}\frac{w_\nu w_\lambda + (\gamma\varepsilon)^2 - \Delta(i\omega_\nu)\Delta(i\omega_\lambda)}{[w_\nu^2-(\gamma\varepsilon)^2-\Delta^2(i\omega_\nu)][w_\lambda^2-(\gamma\varepsilon)^2-\Delta^2(i\omega_\lambda)]}N_{c,0}(\varepsilon)d\varepsilon, \tag{B1}$$

where the shorthand $w_{\nu/\lambda} := i\omega_{\nu/\lambda} - \Sigma(i\omega_{\nu/\lambda})$ is employed again. A similar expression is obtained in the combined cases $\mathbf{k}=\mathbf{k}'=\mathbf{q}+\mathbf{Q}=\mathbf{q}'+\mathbf{Q}$ and $\mathbf{k}=\mathbf{q}+\mathbf{Q}=\mathbf{k}'+\mathbf{Q}=\mathbf{q}'$ for which the momentum through the segment is $\mathbf{Q}$,

$$A_2 = -\frac{2UT}{Z}\sum_{\omega_\nu-\omega_\lambda=\omega_m}\int_{-\infty}^{\infty}\frac{w_\nu w_\lambda - (\gamma\varepsilon)^2 - \Delta(i\omega_\nu)\Delta(i\omega_\lambda)}{[w_\nu^2-(\gamma\varepsilon)^2-\Delta^2(i\omega_\nu)][w_\lambda^2-(\gamma\varepsilon)^2-\Delta^2(i\omega_\lambda)]}N_{c,0}(\varepsilon)d\varepsilon. \tag{B2}$$

The segments which *change* the momentum are very important. The cases $\mathbf{k}=\mathbf{k}'=\mathbf{q}+\mathbf{Q}=\mathbf{q}'$ and $\mathbf{k}=\mathbf{q}+\mathbf{Q}=\mathbf{k}'+\mathbf{Q}=\mathbf{q}'+\mathbf{Q}$ yield together

$$A_3 = -\frac{2UT}{Z}\sum_{\omega_\nu-\omega_\lambda=\omega_m}\int_{-\infty}^{\infty}\frac{w_\nu\Delta(i\omega_\lambda) - w_\lambda\Delta(i\omega_\nu)}{[w_\nu^2-(\gamma\varepsilon)^2-\Delta^2(i\omega_\nu)][w_\lambda^2-(\gamma\varepsilon)^2-\Delta^2(i\omega_\lambda)]}N_{c,0}(\varepsilon)d\varepsilon. \tag{B3}$$

The possible combinations of these cases are naturally generated by powers of the matrix

$$\mathbf{A}:=\begin{pmatrix} A_1 & A_3 \\ A_3 & A_2 \end{pmatrix}. \tag{B4}$$

The sum of all these powers is a geometric series yielding finally

$$\chi = -\frac{2}{U}((1-\mathbf{A})^{-1})_{(1,1)}. \tag{B5}$$

Taking the (1,1) element ensures that the average current-current correlation function is calculated. The prefactor compensates for the fact that the end-vertices do not have the factor $-U/2$ which is incorporated in **A**. Equation (31) is a direct consequence of Eq. (B5). The representation (32) follows from Eqs. (B1), (B2), and (B3) by partial fraction decomposition and integration over the conductivity spectral density using the conductivity Green functions.

Now we turn to Eq. (34). For $\chi^{\mathrm{JJ}}(0)$ we need only A_1 at $i\omega_m=0$ since A_3 vanishes at $i\omega_m=0$ and the factor $1-A_2$ then drops out. For A_1 one obtains

$$A_1 = -\frac{2UT}{Z}\sum_{\nu}\int_{-\infty}^{\infty}\frac{(w_\nu+\gamma\varepsilon)^2-\Delta^2(i\omega_\nu)}{[w_\nu^2-(\gamma\varepsilon)^2-\Delta^2(i\omega_\nu)]^2}N_{c,0}(\varepsilon)d\varepsilon \tag{B6a}$$

$$= -\frac{2UT}{Z}\sum_{\nu}\int_{-\infty}^{\infty}\frac{w_\nu^2-(\gamma\varepsilon)^2-\Delta^2(i\omega_\nu)+2(\gamma\varepsilon)^2}{[w_\nu^2-(\gamma\varepsilon)^2-\Delta^2(i\omega_\nu)]^2} \times N_{c,0}(\varepsilon)d\varepsilon \tag{B6b}$$

$$= -\frac{2UT}{Z}\sum_{\nu}\int_{-\infty}^{\infty}\frac{N_{c,0}(\varepsilon)-\partial(\varepsilon N_{c,0}(\varepsilon))/\partial\varepsilon}{w_\nu^2-(\gamma\varepsilon)^2-\Delta^2(i\omega_\nu)}d\varepsilon \tag{B6c}$$

$$= -\frac{UT}{Z}\sum_{\nu}\int_{-\infty}^{\infty}\frac{\varepsilon^2}{w_\nu^2-(\gamma\varepsilon)^2-\Delta^2(i\omega_\nu)}N_0(\varepsilon)d\varepsilon \tag{B6d}$$

$$= \frac{UT}{\pi Z}\int_{-\infty}^{\infty}f_F(\omega)\,\mathrm{Im}\int_{-\infty}^{\infty}\frac{\varepsilon^2 N_0(\varepsilon)d\varepsilon d\omega}{[\omega-\Sigma(\omega)]^2-(\gamma\varepsilon)^2-\Delta^2(\omega)}. \tag{B6e}$$

The step to Eq. (B6b) follows from the fact that $N_{c,0}(\varepsilon)$ is even. Partial integration of the last term of the numerator leads to Eq. (B6c). Equation (B6d) is obtained using Eq. (29), which emphasizes the importance of this relation between DOS and conductivity spectral density. In the end one obtains

$$A_1 = -\frac{\sqrt{Z}\Sigma^F}{\gamma} \tag{B7a}$$

$$= -\frac{U\langle\hat{T}\rangle}{\gamma Z} \tag{B7b}$$

$$= -(1/\gamma-1). \tag{B7c}$$

One obtains Eq. (34) by substituting Eq. (B7c) in the denominator of Eq. (31) and comparing the resulting expression with Eq. (B7b). This completes the analytic derivation of the f sum rule in the self-consistent $1/d$ approximation, which is considered here.

*Electronic address: uhrig@solrt.lps.u-psud.fr

[1] W. Metzner and D. Vollhardt, Phys. Rev. Lett. **62**, 324 (1989).
[2] D. Vollhardt, in *Correlated Electron Systems*, edited by V. J. Emery (World Scientific, Singapore, 1993), p. 57.
[3] A. Georges, G. Kotliar, W. Krauth, and M. J. Rozenberg, Rev. Mod. Phys. **68**, 13 (1996).
[4] Th. Pruschke, M. Jarrell, and J. K. Freericks, Adv. Phys. **44**, 187 (1995).
[5] E. Müller-Hartmann, Z. Phys. B **74**, 507 (1989).
[6] E. Halvorsen, G. S. Uhrig, and G. Czycholl, Z. Phys. B **94**, 291 (1994).
[7] R. Strack and D. Vollhardt, J. Low Temp. Phys. **84**, 357 (1991).
[8] H. Schweitzer and G. Czycholl, Z. Phys. B **83**, 93 (1991).
[9] V. Janiš and D. Vollhardt, Int. J. Mod. Phys. **6**, 731 (1992).
[10] G. Rickayzen, *Green's Functions and Condensed Matter* (Academic Press, London, 1980).
[11] H. Schweitzer and G. Czycholl, Z. Phys. B **79**, 377 (1990).
[12] G. Baym and L. P. Kadanoff, Phys. Rev. **124**, 287 (1961).
[13] G. Baym, Phys. Rev. **127**, 1391 (1962).
[14] H. Schweitzer and G. Czycholl, Phys. Rev. Lett. **67**, 3724 (1991).
[15] G. S. Uhrig and R. Vlaming, Ann. Phys. **4**, 778 (1995).
[16] The imaginary part is in fact antisymmetric in ω so that one obtains a contradiction by choosing an appropriate sign of ω, too.
[17] H. Schweitzer and G. Czycholl, Solid State Commun. **74**, 735 (1990).
[18] A. Schiller and K. Ingersent, Phys. Rev. Lett. **75**, 113 (1995).
[19] E. Müller-Hartmann, Z. Phys. B **76**, 211 (1989).
[20] B. Menge and E. Müller-Hartmann, Z. Phys. B **82**, 237 (1991).
[21] J. M. Luttinger, Phys. Rev. **121**, 942 (1961).
[22] P. G. J. van Dongen, Phys. Rev. Lett. **67**, 757 (1991).
[23] P. G. J. van Dongen, Phys. Rev. B **50**, 14 016 (1994).
[24] G. D. Mahan, *Many-Particle Physics*, 2nd ed. (Plenum Press, New York, 1990).
[25] A. Khurana, Phys. Rev. Lett. **64**, 1990 (1990).
[26] G. S. Uhrig and D. Vollhardt, Phys. Rev. B **52**, 5617 (1995).
[27] G. S. Uhrig, Physica B **206/207**, 698 (1995).
[28] Th. Pruschke, D. L. Cox, and M. Jarrell, Europhys. Lett. **21**, 593 (1993).
[29] Th. Pruschke, D. L. Cox, and M. Jarrell, Phys. Rev. B **47**, 3553 (1993).
[30] D. Vollhardt and P. Wölfle, *The Superfluid Phases of Helium 3* (Taylor and Francis, London, 1990).
[31] The argument is applied first to finite systems for which the Hilbert space is finite dimensional and the spectra discrete. The theorem's statement extends to the thermodynamic limit if this limit exists.